

Nonequilibrium model of laser-induced phase change processes in amorphous silicon thin films

R. Černý

Department of Physics, Faculty of Civil Engineering, Czech Technical University, Thákurova 7, 166 29 Prague 6, Czech Republic

P. Příkryl

Mathematical Institute, Academy of Sciences of the Czech Republic, Žitná 25, 115 67 Prague 1, Czech Republic

(Received 11 February 1997; revised manuscript received 14 July 1997)

A mathematical model of nonequilibrium phase change processes in amorphous silicon induced by pulsed lasers, which includes explosive crystallization, melting, evaporation, and crystallization from the solid/liquid interface and takes into account the thermophysical properties of polycrystalline silicon in dependence on the grain size, is formulated in the paper. The computational implementation of the model is used to simulate phase changes in a typical case of XeCl excimer laser irradiation of 50 nm to 8 μm thick amorphous silicon layers deposited on the quartz substrate, where characteristic thermal and optical effects accompanying the irradiation process are demonstrated. The experimental verification of the model is discussed, and a comparison of simulated data with experimental measurements of various groups is performed. The model is shown to achieve agreement with experimental data in a variety of experimental situations. It can also be employed to provide estimated values of thermophysical and optical parameters of polycrystalline silicon in dependence on the grain size. [S0163-1829(98)06001-9]

I. INTRODUCTION

In the beginnings of mathematical modeling of phase change processes in amorphous semiconductors, there was a lot of confusion about the values of the thermophysical and optical parameters used. First models (see Refs. 1,2) employed the same thermophysical and optical data for amorphous silicon (*a*-Si) and for the monocrystalline silicon (*c*-Si), and could not explain, for instance, the experimentally measured significantly lower values of the melting onset temperature³ and longer melt duration times⁴ for *a*-Si compared to the *c*-Si specimens.

Webber, Cullis, and Chew⁵ made an important step towards a more correct physical model of *a*-Si melting and found two main reasons of considerable discrepancies between the modeled and experimental data, namely, improper values of thermal conductivity and melting temperature of *a*-Si employed in the previous models. The thermal conductivity values for *a*-Si estimated in Ref. 5 were two orders of magnitude lower than those for *c*-Si as a logical consequence of the disordered structure of *a*-Si and strong phonon scattering, and the melting temperature of *a*-Si was estimated to lie several hundreds of Kelvin under the melting temperature of *c*-Si. The findings of Webber, Cullis, and Chew⁵ about the thermophysical data of *a*-Si were soon confirmed and significantly extended by the measurements and calculations by Lowndes, Wood, and Narayan.⁶

Further experimental investigations of laser-irradiated *a*-Si layers on the *c*-Si bulk using transmission electron microscopy and time-resolved conductivity⁷⁻⁹ revealed the existence of polycrystalline silicon (pc-Si) layers with various structure and grain size which also varied in the depth profile, depending on the energy density of the pulse and initial thickness of the *a*-Si layer. The complicated structure of the pc-Si layers was ascribed to the explosive crystallization

which was observed earlier by Leamy *et al.*¹⁰ for germanium.

The increasing technological interest in pc-Si formed from amorphous layers in the last few years also led to an effort to improve the theoretical knowledge of various states of *a*-Si and its transient phases, and new structural models of *a*-Si appeared (see Refs. 11,12), which made it possible to express the contribution of defects to the thermodynamic properties of *a*-Si, for instance. Owing to the fact how much extensive work on pc-Si has been done in the last few years, it can be anticipated that more precisely formulated transformation mechanisms may appear in the near future.

Mathematical models of laser-induced melting and crystallization of *a*-Si layers which would take into account the real physical properties of pc-Si were formulated only sparsely in the past. The paper by Černý *et al.*¹³ belongs to the very few attempts in this direction. The authors presented here a model which takes variations of the grain size of the resulting pc-Si, depending on the type of the phase change process, into account. The unknown material properties of pc-Si such as the thermal conductivity and phase transition temperatures were obtained as a result of matching the experimentally determined and numerically simulated data of time-resolved reflectivity. However, solely the comparison with the experimental data of the same research group was done here, and no extensions of the numerical model beyond this point were performed.

In this paper, we employ basically the same model as in Ref. 13, with only slight modifications in the physical justification, namely, the explosive crystallization front is defined more correctly as a discontinuity surface representing the thin liquid layer propagating into the *a*-Si layer (we talked about the solid-state crystallization process in this respect in Ref. 13), and the material parameters of pc-Si employed are specified more accurately than in Ref. 13, which was achieved as a result of further optimization work done within

the last two years. Therefore, this paper has two main aims. The first is to demonstrate the ability of the model to simulate a relatively wide range of experimental situations and to give some numerical results which might be useful to the experimentalists, such as the temperature fields, time development of interface positions, and velocities and overheatings/undercoolings. The second is a comparison of our results with independent experimental data measured by other experimental groups and a verification of the model for other experimental situations.

II. PHYSICAL MODEL

The theoretical model of pulsed-laser induced phase change processes in *a*-Si employed in our simulations was briefly described in Ref. 13, but without any detailed physical justification. Therefore, we give some more physical details here. A brief version of the mathematical model already introduced in Ref. 13 is included in the Appendix for the convenience of the reader.

We assume the following mechanism of phase change processes in *a*-Si. The solid material is heated without a phase transition until the surface reaches the temperature which is high enough to initiate melting of a thin layer near the surface. This liquid layer begins to resolidify as pc-Si immediately, and, as the latent heat released during resolidification is higher than that of melting of *a*-Si, the temperature of the newly formed pc-Si layer increases above the melting temperature of *a*-Si. The amorphous material thus begins to melt. However, this new liquid layer is severely undercooled with respect to the pc-Si state and resolidifies immediately as fine grain (FG) pc-Si. This mechanism of phase transitions results in the propagation of a very thin liquid layer through the amorphous material as a result of the difference between the latent heat $L_{m,a}$ of melting of *a*-Si and the latent heat L_{pc} of crystallization of pc-Si. This process is called explosive crystallization (XC).

The absorption of the laser energy near to the surface of the sample leads to a further fast increase of the surface temperature of pc-Si, which reaches the melting temperature of pc-Si soon. Thus, a phase interface between *l*-Si and pc-Si appears which moves into the sample. With the temperature increase of the surface due to the intensive absorption of laser energy in the liquid, as compared with that in the solid material, the evaporation from the surface may become important as well.¹⁴

In the mathematical formulation of explosive crystallization, we utilize the fact that the propagating liquid layer is very thin, and replace it by a discontinuity surface where the difference between the latent heat of crystallization of pc-Si and the latent heat of melting of *a*-Si, $L_{XC} = L_{pc} - L_{m,a}$, is released. In what follows, this discontinuity surface will be called the XC front. The process of XC has a nonequilibrium character as it is quite apparent that the temperature of the thin liquid layer depends on its propagation velocity which is proportional to the amount of heat released during XC. Therefore, we employ a nonequilibrium model in describing the movement of the XC front, and introduce an ‘‘equilibrium explosive crystallization temperature’’ T_{XC} at which the velocity of the XC front is equal to zero.

Further surface temperature increase, due to both absorp-

tion of laser light and release of L_{XC} , leads to the melting of the FG pc-Si layer formed by XC, which is modeled in a similar way as the melting of monocrystalline silicon (see Ref. 15 for details). We employ a nonequilibrium model of pc-Si/*l*-Si phase transition here as well and introduce the equilibrium melting temperature of pc-Si, $T_{m,pc}$, defined as the temperature at which the pc-Si/*l*-Si interface velocity is equal to zero.

The vaporization from the surface, which takes place at sufficiently high temperatures, is modeled using a simple kinetic theory of evaporation into vacuum as most of the experimental work is performed under vacuum conditions. This process can also be considered as a nonequilibrium one in the sense of how the nonequilibrium processes in the other phase transitions were defined since the vapor pressure is a function of the surface temperature T_s , and therefore the interface velocity is a function of T_s as well.

When the position of the *l*-Si/pc-Si interface reaches its maximum value, the melting process stops due to the decrease of the absorbed laser energy, and the crystallization from the *l*-Si/pc-Si interface begins. The grain size of the newly formed pc-Si may differ from that of pc-Si bulk since the process may be running at a different temperature and a different velocity of the interface than XC. Therefore, the values of thermal conductivity, density, and specific heat may be different from those used before. Also, the latent heat of crystallization, L_{pc} , released during this process need not be generally equal to the latent heat of melting of pc-Si, $L_{m,pc}$, and, similarly, the equilibrium temperature of the *l*-Si→pc-Si transition need not be generally equal to that of the opposite phase transition. The newly formed pc-Si described above will be called large grain (LG) pc-Si.

Eventually, the *l*-Si/pc-Si interface reaches the surface and the crystallization is completed. In the general case, we then arrive at the following structure of the sample: just below the surface, in $[Z_{0,fin}, Z_{1,max}]$, where $Z_{0,fin}$ is the final position of the surface, $Z_{1,max}$ is the maximum thickness of the molten layer, we have the secondary pc-Si layer created from the melt pool. The underlying primary pc-Si layer originating from the explosive crystallization, which can generally have a different grain size, occupies the region $[Z_{1,max}, Z_{2,max}]$, where $Z_{2,max}$ is the final position of the XC front. The remaining *a*-Si and the substrate (usually quartz) lie beyond $Z_{2,max}$.

III. NUMERICAL SIMULATIONS

The computational implementation of the mathematical model was done using the Galerkin finite element method (see, e.g., Ref. 16), and a computer code in FORTRAN 77 was developed. In the numerical calculations, we simulated the irradiation of *a*-Si layers on fused quartz substrate by an XeCl laser [28 ns full width at half maximum (FWHM), 308 nm]. The initial thickness of the *a*-Si layer A varied from 50 to 8000 nm, the laser energy density E was in the range $[0.05 - 1.00 \text{ J cm}^{-2}]$.

The material parameters of *l*-Si and *a*-Si in our mathematical model (see Appendix) were taken from the following sources: (a) c_l from Ref. 17, (b) ρ_l and all the optical parameters of *l*-Si from Ref. 18, (c) $K_l(T)$ from Ref. 19, (d) the parameters A, B, C from Ref. 20, (e) L_v from Ref. 21, (f)

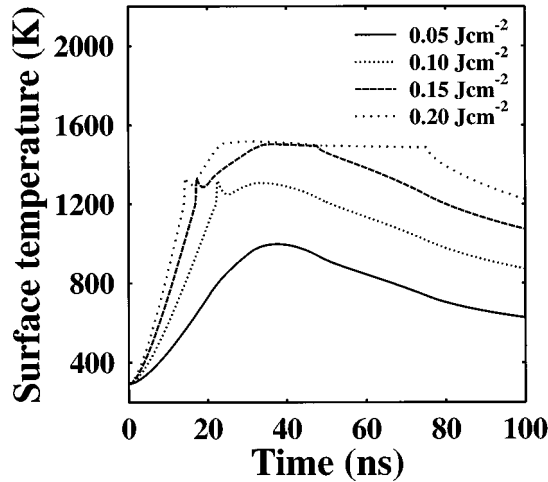


FIG. 1. Time histories of the surface temperatures for $A = 100$ nm and various energy densities.

K_a and c_a from Ref. 5, (h) ρ_a from Ref. 22, (i) the refraction index $n_a(T)$ and the extinction coefficient $k_a(T)$ from Ref. 9, (j) $L_{m,a}$ from Ref. 23.

Since, to our knowledge, no analogous data for pc-Si have been published in the open literature, we had to use estimated values in the model calculations. We assumed the density and specific heat of pc-Si to be equal to the values of monocrystalline Si and took them from Ref. 17, the same approximation was also used for the refraction index and the extinction coefficient at 308 nm and the data were taken from Ref. 18. For n_{pc} and k_{pc} at 633 nm of FG and LG pc-Si, the estimates by Lowndes *et al.*⁹ were used. For the coefficients C_1 , C_2 of the interface response functions from Eqs. (A6), (A8), we took the measured values for pc-Si from Ref. 24 and for a -Si from Ref. 25, respectively. The equilibrium explosive crystallization temperature T_{XC} was chosen to be equal to the melting temperature of as-implanted a -Si from Ref. 26, $T_{XC} = 1200$ K. The remaining material parameters, K_{pc} , L_{pc} , and L_{XC} , which may also change with the varying grain size of pc-Si, were determined by a fitting procedure with the model described in the Appendix. The main criterion in our fitting procedure was to achieve the agreement with the experimental data in the melt durations²⁷ within the margin of $\pm 5\%$. The results of our fitting procedure can be summarized as follows. In the XC phase, we obtained for the FG pc-Si $L_{XC} = 185$ J/g, $L_{pc} = L_{XC} + L_{m,a} = 1505$ J/g, $K_{pc} = 0.05$ W/cmK, $T_{pc} = 1500$ K, while for the LG pc-Si formed by the crystallization from the melt pool we have $L_{pc} = 1700$ J/g, $K_{pc} = 0.10$ W/cmK, $T_{pc} = 1500$ K.

The evaluation of our computational experiments can be conveniently split in two basic parts characterizing the influence of the two most important parameters of the process, the pulse energy density E and the initial thickness of the a -Si layer A . For the illustration of the influence of E on the basic characteristic parameters of the process (such as the temperature field, interface positions and velocities, melt duration, etc.) we have chosen $A = 100$ nm which is a usual experimental value.

Figure 1 shows the time histories of the surface temperatures $T_s(t)$ for low values of E . The explosive crystallization threshold $E_{XC} = 0.10$ J cm⁻² can be clearly distinguished in

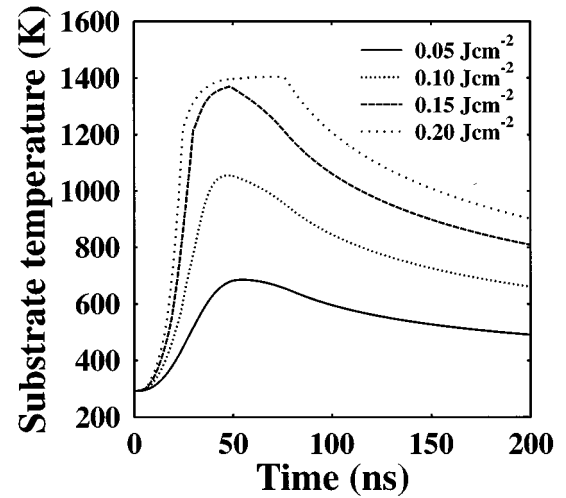


FIG. 2. Time histories of the substrate temperatures for $A = 100$ nm and various energy densities.

the figure. The sharp peaks in the first part of the $T_s(t)$ curves for $E \geq 0.10$ J cm⁻² correspond to the onset of explosive crystallization, which is accompanied by a fast release of latent heat contributing temporarily in the near-surface region to the main heat source, which is the absorption of laser light.

The histories of the substrate temperatures in Fig. 2 can help us to monitor the extent of the phase change processes in the thin silicon layer. We can see here that for $E \geq 0.15$ J cm⁻² the whole a -Si layer underwent explosive crystallization to pc-Si during the pulse as the substrate surface temperature exceeded T_{XC} . The development of the explosive crystallization in the a -Si film is illustrated in Fig. 3 more clearly, where the histories of the XC front position are plotted in dependence on the energy density.

Figure 4 shows the velocities of the XC front for low values of E and provides additional information on the heat transfer in the thin film. The first peak corresponds to the simultaneous heat release due to both laser light absorption and explosive crystallization, which was previously men-

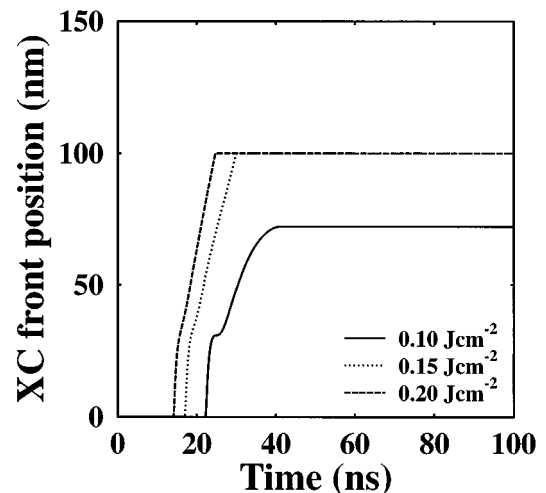


FIG. 3. Dependence of the position of the XC front on the energy density for $A = 100$ nm.

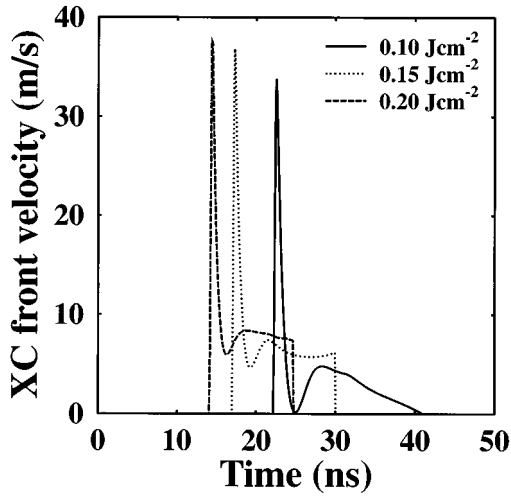


FIG. 4. Dependence of the velocity of the XC front on the energy density for $A = 100$ nm.

tioned. The sudden decrease of interface velocities following this peak is due to the fact that the XC front quickly moves deeper into the film and the latent heat release is shifted somewhere into the region near to the absorption length of the XeCl laser ($l_{\text{pc-Si}} \approx 42$ nm), where the intensity of laser light absorption significantly decreases. This is also documented by the small step in the increasing part of the XC front position vs time curve for $E = 0.10$ J cm $^{-2}$ in Fig. 3, which roughly equals the value of $l_{\text{pc-Si}}$. Below $l_{\text{pc-Si}}$, heat conduction together with the release of latent heat become the only heating mechanisms, the movement of the crystallization front slows thus down, and later stops as the heat sources are insufficient to keep the interface temperature above T_{XC} .

Figure 5, showing the positions of the pc-Si/l-Si interface, can help us to identify the melting threshold E_m , which for the chosen value of the initial thickness of the a -Si layer was $E_m = 0.15$ J cm $^{-2}$. This can also be observed in Fig. 1 where a small plateau appears at about 1500 K on the $T_s(t)$

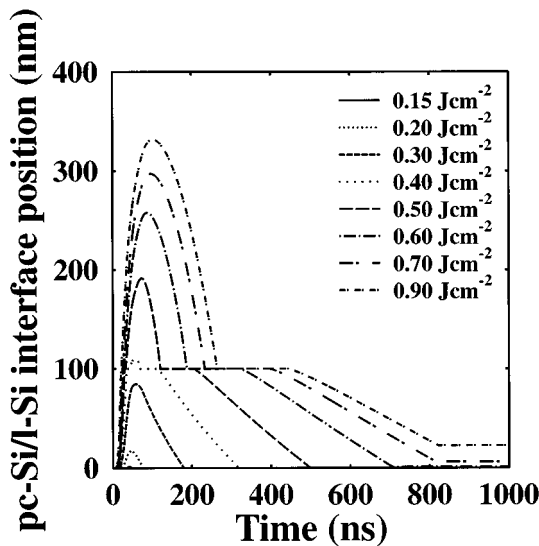


FIG. 5. Dependence of the position of the pc-Si/l-Si interface on the energy density for $A = 100$ nm.

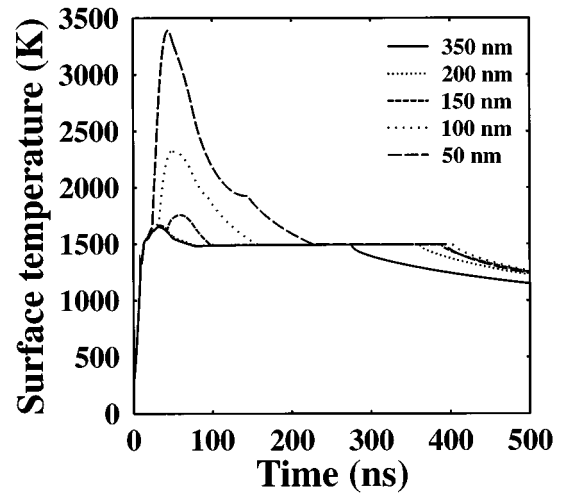


FIG. 6. Time histories of the surface temperatures for $E = 0.45$ J/cm 2 and the initial thickness of a -Si layer $A \in [50$ nm, 350 nm].

curve for the energy density $E = E_m$. For $E \geq 0.40$ J cm $^{-2}$, the maximum thickness of the molten layer exceeds A , and therefore the quartz substrate melts. In Fig. 5, it may also be seen that for $E \geq 0.60$ J cm $^{-2}$ the final parts of the $Z_1(t)$ curves do not coincide with zero. This is a consequence of the increasing role of evaporation for higher laser energies.

The influence of the initial thickness of the a -Si layer A on the course of the phase change processes is shown in the second group of figures for the energy density $E = 0.45$ J/cm 2 .

Figure 6 shows the surface temperatures for low values of A . The temperature maxima increase significantly with decreasing A for $A < 150$ nm. This fact can be explained using the histories of pc-Si/l-Si interface positions in Fig. 7 showing that for $A < 150$ nm the quartz substrate melts. The melting temperature of quartz is higher than that of silicon, and therefore the entire process takes place at higher tempera-

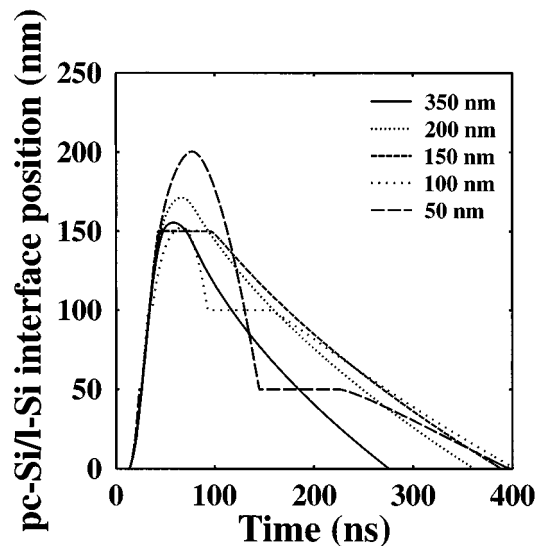


FIG. 7. Dependence of the position of the pc-Si/l-Si interface on the a -Si layer thickness for $E = 0.45$ J/cm 2 .

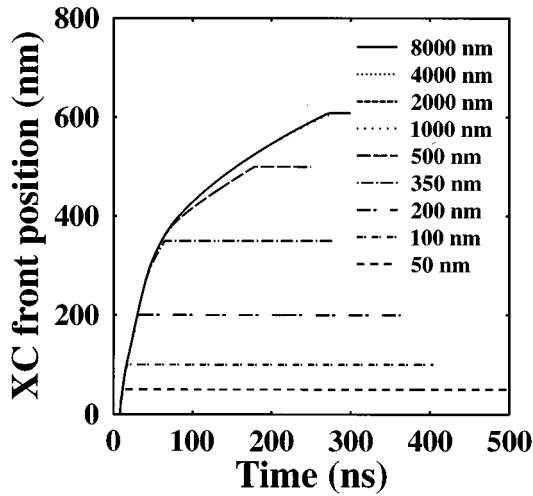


FIG. 8. Dependence of the position of the XC front on the a -Si layer thickness for $E=0.45 \text{ J/cm}^2$.

tures. In addition, the latent heat of melting of quartz is approximately seven times lower than that of pc-Si and more laser energy absorbed in the material can be spent for heating the liquid. The logical consequence is the fast temperature increase in the liquid documented in Fig. 6. This explanation is also supported by Fig. 7 showing that the maximum thickness of the molten layer does not increase dramatically with decreasing A despite the low latent heat of melting of quartz.

The computational results for higher a -Si layer thicknesses show that the surface temperature histories are unaffected by the initial a -Si layer thickness for $A > 1000 \text{ nm}$ and the substrate temperatures become independent of A for $A > 2000 \text{ nm}$. The value of $A = 1000 \text{ nm}$ is roughly consistent with the heat-diffusion length

$$l_H = \sqrt{\frac{K}{\rho c} t_p}$$

where t_p is the time interval ($t_p \approx 500 \text{ ns}$), which is $\sim 1100 \text{ nm}$ for pc-Si and $\sim 3000 \text{ nm}$ for l -Si (the maximum thickness of the molten layer is $\sim 150 \text{ nm}$ for these values of A). The difference in the limiting values of A for the substrate and for the surface temperatures can be explained by the release of latent heat during XC deeper in the layer. Figure 8 shows that the explosive crystallization front always reaches the substrate surface for $A \leq 500 \text{ nm}$, whereas for $A \geq 1000 \text{ nm}$ it stops at about $Z_2 = 600 \text{ nm}$. Therefore, for higher values of A the deeper layers are heated only by the heat conduction which is slower in a -Si and quartz than in pc-Si. Taking into account that in this case the heat-diffusion length for a -Si is $\sim 500 \text{ nm}$, it can be stated that also the substrate temperatures are consistent with the concept of heat-diffusion length as for $A = 1000 \text{ nm}$ we have $A - Z_2 \approx 400 \text{ nm}$, which is still within l_H , while for $A = 2000 \text{ nm}$ we have $A - Z_2 \approx 1600 \text{ nm}$, which is already three times larger than l_H .

Regarding the study of the dependence of other important parameters on the initial thickness of the a -Si layer A , our calculations showed that both the explosive crystallization and melting threshold were basically independent of A . The

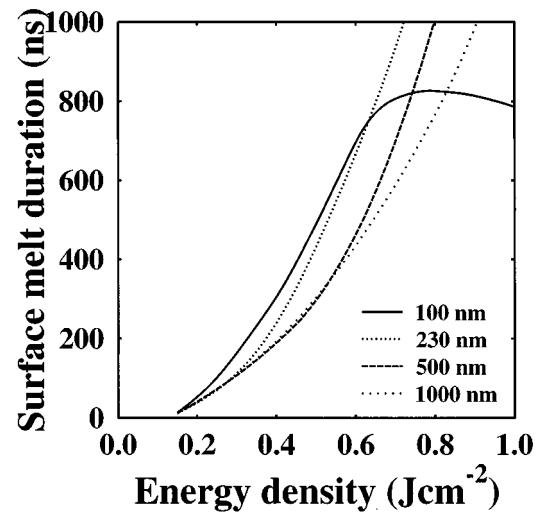


FIG. 9. Melt duration as a function of energy density E and initial thickness of the a -Si layer A .

main reason for this behavior lies in the fact that the thermal conductivities of a -Si and quartz are apparently very similar.

It is useful to know some of the characteristic parameters of the process in dependence on both the energy density E and the initial thickness of the a -Si layer A , mainly for technological reasons. To these parameters, the melt duration t_m shown in Fig. 9 belongs, for instance.

In the region of low-energy densities, $E \leq 0.60 \text{ J cm}^{-2}$, the surface melt duration increases with decreasing A generally. However, we can see that the $t_m(E)$ curve for $A = 100 \text{ nm}$ is above the remaining ones in the whole range of low-energy densities, while the curves for $A = 230$ and 500 nm almost coincide for $E \leq 0.30 \text{ J cm}^{-2}$, and those for $A = 500$ and $A = 1000 \text{ nm}$ coincide even up to $\sim 0.60 \text{ J cm}^{-2}$. This fact can be explained by the extent of explosive crystallization. For a low A , the explosive crystallization is finished very fast (see Fig. 8) because the whole a -Si layer is crystallized; for higher A it takes logically a longer time. The thickness of the pc-Si layer is then the decisive factor for heat transfer in the heating phase as the thermal conductivity of pc-Si is several times higher than that of the quartz substrate. Consequently, in a certain range of energy densities, for low values of A the quartz substrate prevents the fast heat removal from the near-surface region, the temperature in this region increases, the melting process is faster (see Fig. 7), and also surface melt duration is longer.

For $E \geq 0.60 \text{ J cm}^{-2}$, the situation is changed. We can see that the $t_m(E)$ curve for $A = 100 \text{ nm}$ loses its increasing character and the melt duration begins even to decrease slowly with E increasing. The main reason for this behavior can be found in the increasing effect of evaporation. As the latent heat of evaporation of Si is approximately eight times higher than the latent heat of melting of a -Si, the evaporation process is very demanding energetically and a substantial part of laser energy is spent for evaporation. In a combination with the low thermal conductivity of the quartz substrate this results in slowing down the melting process, which for these laser energies and in the key time interval of ~ 50 to $\sim 100 \text{ ns}$, when evaporation is most important, occurs deep in the quartz substrate (Fig. 5).

IV. DISCUSSION

Numerical experiments with pulsed-laser-induced phase change processes in amorphous silicon can provide information about some parameters which cannot be obtained experimentally. Among these, the temperature fields and the interface velocities are the most important. On the other hand, the lack of appropriate experimental data makes the verification of the model more complicated.

In the laser-controlled processes where phase changes take place, the most frequently used experimental techniques which might lead to results directly comparable with computational models are the time-resolved reflectivity (TRR) and time-resolved conductivity (TRC) measurements. TRR measurements can be simulated numerically with only slight modifications of our mathematical model. It is sufficient just to modify the procedure for calculating the reflectivity of the primary laser (see Appendix) for the wavelength of the probe laser beam (a HeNe laser, 633 nm, in most experimental setups). The simulation of TRC measurements is also straightforward. It consists in utilizing the Kirchhoff Laws together with the calculated melt depths and temperature fields. Both TRR and TRC provide similar information and they can identify the appearance and duration of the molten phase. The measured melting thresholds and melt durations can then be compared with the numerical results.

TRR measurements may also help us to identify the appearance of pc-Si after transformation from the amorphous phase since the optical properties of *a*-Si and pc-Si differ significantly. Under these conditions, the jump changes of the complex refractive index in the region just below the sample surface can lead to substantial additional reflections which are well within the detection limits.

In mathematical modeling of processes where various silicon phases appear, it is necessary to take into account the significant uncertainty in the thermophysical data that depend on the grain size, which may not be known with a sufficient accuracy. It was already mentioned in the beginning of the previous section that some of the pc-Si data for our model were obtained by a fitting procedure on the basis of our experimental TRR data. These data need not generally characterize all situations which can appear in the laser irradiation of *a*-Si because the final grain size might depend on energy density and initial *a*-Si layer thickness, and possibly also on the substrate.

Therefore, the application of our model to the experimental setups which differ from that of Ref. 13 significantly, i.e., for other substrates, other lasers, etc., should be accompanied by repeating the fitting procedure to get appropriate thermophysical data.

We will illustrate such an application of our model to different experimental conditions for the experimental data of Im, Kim, and Thompson²⁸ which were obtained for *a*-Si layers of thickness 100 nm deposited onto oxidized Si substrates with 100 nm thick SiO₂ layer, and almost the same XeCl excimer laser (30 ns FWHM, 308 nm) as in our numerical experiments.

Figure 10 shows the simulated TRR curves for $A = 100$ nm and low-energy densities. All curves clearly exhibit the initial oscillations indicating the explosive crystallization observed experimentally in Ref. 28 and also the

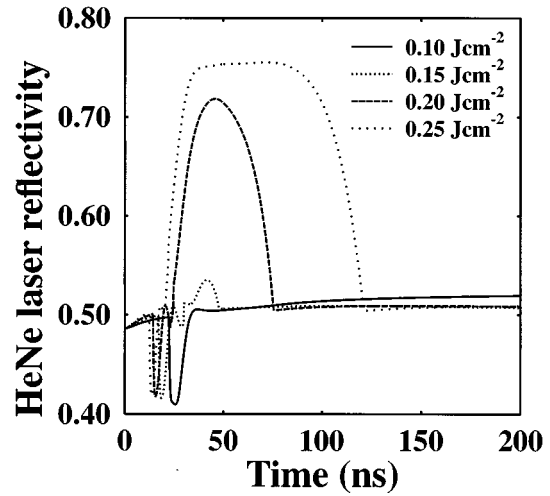


FIG. 10. Simulated TRR curves for HeNe probe laser beam and $A = 100$ nm.

shape of the curves is in good qualitative agreement with the experimental TRR curves from Ref. 28. Also, the melting threshold $E_m = 0.15$ J/cm² obtained in our numerical experiments is in very good agreement with the measured value from Ref. 28, which was $E_m = 0.16$ J/cm².

We achieved, however, very poor agreement in the melt durations t_m as shown in Fig. 11, which is not very surprising as the explosive crystallization front reaches the substrate surface already at $E_m = 0.15$ J/cm² and after that the differences in the thermophysical properties of the substrate must become important.

Therefore, we performed the numerical experiments with exactly the same substrate as in Ref. 28. However, also in this case the differences in melt durations were still remarkable, typically 20–30% for most energy densities as shown in Fig. 11. As we already noted, one of the possible reasons for this might be the difference in the grain size of pc-Si

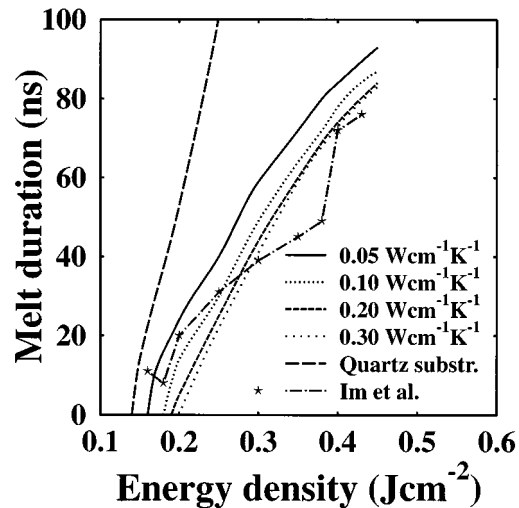


FIG. 11. Calculated melt duration as a function of laser energy density for the oxidized silicon substrate as in Ref. 28 and various values of thermal conductivity of pc-Si, compared to the experimental data of Im, Kim, and Thompson (Ref. 28) and to the calculations with the quartz substrate.

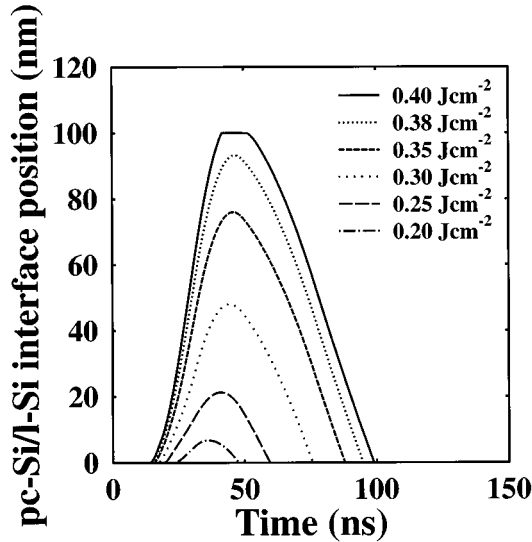


FIG. 12. Calculated position of the pc-Si/l-Si interface for the oxidized silicon substrate as in Ref. 28 and $E \in [0.20 \text{ J/cm}^2, 0.40 \text{ J/cm}^2]$, $K_{pc} = 0.05 \text{ W cm}^{-1} \text{ K}^{-1}$.

between the experiments done by Cháb²⁷ (which were employed for fitting the thermophysical properties) and those performed by Im, Kim, and Thompson.²⁸ Hence, we also show three additional $t_m(E)$ curves in Fig. 11 calculated for higher thermal conductivities of pc-Si, $K_{pc} = 0.10 \text{ W/cm K}$, 0.20 W/cm K , and 0.30 W/cm K . Least-squares based comparisons of experimental ($t_{m,e,i}$) and calculated ($t_{m,i}$) melt durations show that the representative deviation $D_{K_{pc}} = 1/n \sqrt{\sum_{i=1}^n (t_{m,i} - t_{m,e,i})^2}$ is really better for $K_{pc} = 0.10 \text{ W/cm K}$ than for $K_{pc} = 0.05 \text{ W/cm K}$ ($D_{0.10} = 4.08$, $D_{0.05} = 6.31$) but remains almost the same for $K_{pc} = 0.20 \text{ W/cm K}$ ($D_{0.20} = 4.01$), since the computations with $K_{pc} = 0.10 \text{ W/cm K}$ achieve better agreement with experiments for low E ($E \leq 0.25 \text{ J/cm}^2$), while those with $K_{pc} = 0.20 \text{ W/cm K}$ are better for higher E . Calculations with $K_{pc} = 0.30 \text{ W/cm K}$ (which is almost equal to the high-temperature thermal conductivity of monocrystalline silicon) resulted in only slight differences as compared with those for $K_{pc} = 0.20 \text{ W/cm K}$ ($D_{0.30} = 4.55$).

The sudden increase of melt duration between $E = 0.38 \text{ J/cm}^2$ and $E = 0.40 \text{ J/cm}^2$ observed in the experiments of Im, Kim, and Thompson²⁸ could not be reproduced by any simple data fitting in our model. To explain this fact we employ the calculated pc-Si/l-Si interface position histories depicted in Fig. 12, where it is shown that for $E = 0.40 \text{ J/cm}^2$ the melt front reaches the substrate surface and the whole Si layer is fully melted. This confirms well the hypothesis of Im, Kim, and Thompson²⁸ that the range of energy densities just below $E = 0.40 \text{ J/cm}^2$, where this sudden change of t_m appears, is the region of near-complete melting of the film. As the unmelted Si film can no longer be considered as a continuous layer in this situation and significant lateral growth may occur due to the existence of small solid seeds near to the substrate,²⁸ the one-dimensional model employed in this paper cannot be applied successfully to reproduce experimental data in this case.

As follows from the physical and mathematical formulation of the model described in this paper, it has two main

limiting features generally: it is constructed as one-dimensional and assumes the solidification of the melt pool only in the form of crystallization from the phase interface.

The one dimensionality originates from the physical situation in most experimental setups for laser irradiation of semiconductors: the laser spot has the area of several mm^2 , while the laser-affected depth usually does not exceed several μm . For well homogeneous laser beams used in recent experiments it looks like a reasonable approximation. However, for the situations where a remarkable lateral growth can be initiated, as were those in Ref. 28, this approximation is no longer valid.

The solidification from the interface is a good approximation for the processes where the undercooled liquid does not stay at the low temperatures long enough for initiating the nucleation process. This need not be true for instance in the region of high-energy densities, where the l-Si layer can stay at the undercooled temperatures for several hundreds of nanoseconds, which may be sufficient for starting nucleation.

It has been shown experimentally (see Refs. 29,30), also that heterogeneous nucleation can appear in certain situations, which can result in the solidification from the surface, where it is initiated at the residual impurities. Nor is this situation included in our model, which does not take any form of nucleation into account.

V. CONCLUSION

The nonequilibrium mathematical model of laser-induced phase change processes in a-Si thin films formulated in this paper can describe explosive crystallization, melting, evaporation, and solidification from the solid/liquid interface.

The model can reproduce a variety of experimental data measured at laser irradiation of amorphous silicon layers, such as the explosive crystallization threshold, melting, threshold, surface melt duration, and maximum thickness of the molten layer for various experimental setups. It can also provide some data which cannot be obtained experimentally although they are very important both for experimentalists and theoretical physicists, e.g., the temperature field in the layer, the time history of melting, and solidification velocities and the temperature of the phase interfaces.

Although the application of the model is limited to the homogeneous phase change processes which can be considered in the one-dimensional approximation and the model does not take nucleation effects into account, it has been shown that it can achieve a good agreement with measured data in a variety of experimental situations.

In connection with experimental data from TRR and TRC measurements, the model is also capable of providing reasonable estimates of such not commonly measured thermo-physical and optical parameters of pc-Si layers as are the thermal conductivity, latent heat of solidification, and reflectivity in dependence on the grain size.

ACKNOWLEDGMENTS

This research has been supported by the Grant Agency of the Academy of Sciences of the Czech Republic, under Grant No. A1010719 and by the Grant Agency of the Czech Republic, under Grant No. 201/97/0217.

APPENDIX A: MATHEMATICAL MODEL

The mathematical model of phase change processes in a -Si employed in this paper can be formulated in the following way (see Ref. 13):

Supposing the one-dimensional heat conduction to be the dominant mode of energy transfer (see Refs. 15,31 for a detailed justification of this treatment), we can write the energy balance in the form

$$\rho_i c_i \frac{\partial T_i}{\partial t} = \frac{\partial}{\partial x} \left(K_i \frac{\partial T_i}{\partial x} \right) + S_i(x, t), \quad i = l, \text{pc}, a, sb, \quad (\text{A1})$$

where ρ is the density, c the specific heat, T the temperature, K the thermal conductivity, the indices pc, a, l mean the polycrystalline, amorphous and liquid phases, respectively, the index sb means the substrate (usually fused quartz).

The volume heating term S_i arising due to the laser irradiation can be expressed in the form¹⁵

$$S_i(x, t) = [1 - R(t)] \alpha(x) I_0(t) \times \exp \left(- \int_{Z_0(t)}^x \alpha(\eta) d\eta \right), \quad (\text{A2})$$

where $I_0(t)$ is the power density of the pulse (power per unit area), $\alpha = \alpha(x)$ is the optical absorption coefficient, $R = R(t)$ is the reflectivity calculated using the known values of the refractive indices n_i and extinction coefficients k_i (which are temperature dependent) according to the procedure described in Ref. 32, and $Z_0(t)$ is the time-dependent position of the surface of the sample (liquid/vapor interface).

The heat balance condition on the liquid/vapor interface can be expressed as

$$\rho_l L_v \frac{dZ_0}{dt} = K_l \left(\frac{\partial T_l}{\partial x} \right)_{x=Z_0(t)_+} - \epsilon \sigma_{\text{SB}} (T_{Z_0}^4 - T_e^4), \quad (\text{A3})$$

where L_v is the latent heat of evaporation, ϵ is the emissivity from the liquid surface, σ_{SB} is the Stefan-Boltzmann constant, T_{Z_0} is the temperature of the liquid/vapor interface, and T_e is the temperature of the surroundings. The kinetic theory of evaporation into vacuum yields the condition³³

$$\frac{dZ_0}{dt} = \frac{1}{\rho_l} \sqrt{\frac{M}{2\pi R_g}} T_{Z_0}^{C-0.5} \times 10^{-(A/T_{Z_0})+B}, \quad (\text{A4})$$

where R_g is the universal gas constant, M is the molar mass, and A, B, C are constants determined experimentally.

On the pc-Si/ l -Si interface we have the heat balance condition

$$\rho_{\text{pc}} L_{m, \text{pc}} \frac{dZ_1}{dt} = K_{\text{pc}} \left(\frac{\partial T_{\text{pc}}}{\partial x} \right)_{x=Z_1(t)_+} - K_l \left(\frac{\partial T_l}{\partial x} \right)_{x=Z_1(t)_-}, \quad (\text{A5})$$

where $L_{m, \text{pc}}$ is the latent heat of melting of pc-Si, $Z_1(t)$ the position of the pc-Si/ l -Si interface, and the kinetic condition can be expressed schematically in the form

$$\frac{dZ_1}{dt} = C_1 (T_{Z_1} - T_{m, \text{pc}}), \quad (\text{A6})$$

where T_{Z_1} is temperature of the pc-Si/ l -Si interface, C_1 is a constant, and $T_{m, \text{pc}}$ is understood as the equilibrium melting temperature of pc-Si.

Finally, on the XC front we can write the conditions

$$\rho_a L_{\text{XC}} \frac{dZ_2}{dt} = K_{\text{pc}} \left(\frac{\partial T_{\text{pc}}}{\partial x} \right)_{x=Z_2(t)_-} - K_a \left(\frac{\partial T_a}{\partial x} \right)_{x=Z_2(t)_+}, \quad (\text{A7})$$

$$\frac{dZ_2}{dt} = C_2 (T_{Z_2} - T_{\text{XC}}) \geq 0, \quad (\text{A8})$$

where L_{XC} is the heat released during explosive crystallization (see the description of the physical model), $Z_2(t)$ is the position of the XC front, T_{Z_2} is the temperature of the XC front, C_2 is a constant, and T_{XC} is the equilibrium crystallization temperature. The velocity dZ_2/dt of the XC front is assumed to be always positive because the character of XC described in the paper excludes the reverse transition from pc-Si to a -Si in this way. The other boundary conditions and initial conditions are formulated in a standard way according to the experimental setup.

¹P. Baeri, S. U. Campisano, G. Foti, and E. Rimini, J. Appl. Phys. **50**, 788 (1979).

²R. F. Wood and G. E. Giles, Phys. Rev. B **23**, 2923 (1981).

³A. G. Cullis, H. C. Weber, and N. G. Chew, Appl. Phys. Lett. **36**, 547 (1980).

⁴A. Bhattacharyya, B. G. Streetman, and K. Hess, J. Appl. Phys. **52**, 3611 (1981).

⁵H. C. Webber, A. G. Cullis, and N. G. Chew, Appl. Phys. Lett. **43**, 669 (1983).

⁶D. H. Lowndes, R. F. Wood, and J. Narayan, Phys. Rev. Lett. **52**, 561 (1984).

⁷M. O. Thompson, G. J. Galvin, J. W. Mayer, P. S. Peercy, J. M. Poate, D. C. Jacobson, A. G. Cullis, and N. G. Chew, Phys. Rev. Lett. **52**, 2360 (1984).

⁸W. Sinke and F. W. Saris, Phys. Rev. Lett. **53**, 2121 (1984).

⁹D. H. Lowndes, S. J. Pennycook, G. E. Jellison, Jr., S. P. Withrow, and D. N. Mashburn, J. Mater. Res. **2**, 648 (1987).

¹⁰H. J. Leamy, W. L. Brown, G. K. Celler, G. Foti, G. H. Gilmer, and J. C. C. Fan, Appl. Phys. Lett. **38**, 137 (1981).

¹¹P. A. Stolk, F. W. Saris, A. J. M. Berntsen, W. F. van der Weg, L. T. Sealy, R. C. Barklie, G. Krötz, and G. Müller, J. Appl. Phys. **75**, 7266 (1994).

¹²Y. Masaki, M. Suzuki, and A. Kitagawa, J. Appl. Phys. **77**, 1766 (1995).

¹³R. Černý, V. Vydra, P. Příkryl, I. Ulrych, J. Kočka, K. M. A. El-Kader, Z. Chvoj, and V. Cháb, Appl. Surf. Sci. **86**, 359 (1995).

¹⁴R. Černý and P. Příkryl, Z. Angew. Math. Mech. **74**, 568 (1994).

¹⁵R. Černý, R. Šášík, I. Lukeš, and V. Cháb, Phys. Rev. B **44**, 4097 (1991).

- ¹⁶O. C. Zienkiewicz, *The Finite Element Method in Engineering Science* (McGraw-Hill, London, 1971).
- ¹⁷P. D. Desai, *J. Phys. Chem. Ref. Data* **15**, 967 (1986).
- ¹⁸S. de Unamuno and E. Fogarassy, *Appl. Surf. Sci.* **36**, 1 (1989).
- ¹⁹R. F. Wood and G. E. Jellison, in *Pulse Laser Processing of Semiconductors*, edited by R. F. Wood, C. W. White, and R. T. Young (Academic, Orlando, 1984), p. 165.
- ²⁰S. Dushman, *Scientific Foundations of Vacuum Technique* (Wiley, New York, 1962).
- ²¹H. Landolt and R. Börnstein, *Numerical Data and Functional Relationships in Science and Technology* (Springer-Verlag, Berlin, 1982), Vol. 17.
- ²²J. S. Custer, M. O. Thompson, D. C. Jacobson, J. M. Poate, S. Roorda, W. C. Sinke, and F. Spaepen, *Appl. Phys. Lett.* **64**, 437 (1994).
- ²³E. P. Donovan, F. Spaepen, D. Turnbull, J. M. Poate, and D. C. Jacobson, *Appl. Phys. Lett.* **42**, 698 (1983).
- ²⁴X. Xu, C. P. Grigoropoulos, and R. E. Russo, *Appl. Phys. Lett.* **65**, 1745 (1994).
- ²⁵D. H. Lowndes, G. E. Jellison, Jr., S. J. Pennycook, S. P. Withrow, and D. N. Mashburn, *Appl. Phys. Lett.* **48**, 1389 (1986).
- ²⁶P. Stolk, Ph.D. thesis, Universiteit Utrecht, 1993.
- ²⁷V. Cháb (unpublished).
- ²⁸J. S. Im, H. J. Kim, and M. O. Thompson, *Appl. Phys. Lett.* **63**, 1969 (1993).
- ²⁹S. U. Campisano, D. C. Jacobson, J. M. Poate, A. G. Cullis, and N. G. Chew, *Appl. Phys. Lett.* **45**, 1217 (1984).
- ³⁰S. U. Campisano, D. C. Jacobson, J. M. Poate, A. G. Cullis, and N. G. Chew, *Appl. Phys. Lett.* **46**, 846 (1985).
- ³¹R. Černý, I. Lukeš, V. Cháb, and R. Šášik, *Thermochim. Acta* **218**, 173 (1993).
- ³²M. Born and E. Wolf, *Principles of Optics* (Pergamon, Oxford, 1991).
- ³³R. Černý and Y. Bayazitoglu, *Num. Heat Transfer A* **25**, 135 (1994).